=== **SOLID STATE** ===

Nonlinear Dynamics of Deformation Bands in Aluminum−Magnesium Alloy in the Creep Test

A. A. Shibkov*, M. A. Zheltov, M. F. Gasanov, and A. E. Zolotov

Derzhavin State University, Tambov, 392000 Russia
e-mail: shibkov@tsu.tmb.ru
Received January 31, 2017

Abstract—Various types of plastic instabilities that emerge in intermittent creep have been studied experimentally for AlMg6 aluminum−magnesium alloy. It has been shown that intermittent creep exhibits threshold dynamics. The deformation step on the creep curve of amplitude is ~1−6% and begins when the rate of the preceding continuous creep attains a certain critical value. In the course of evolution of the step, the strain rate varies in the interval that spans more than two orders of magnitude, and transitions occur between different dynamic regimes of type *A* and *B* characterized by different stress drop regularity levels in the force response. Nonlinear aspects of the deformation behavior of the alloy in the intermittent creep conditions are considered.

INTRODUCTION

In recent years, intermittent deformation has drawn the attention of researchers as an example of the complexity of the spatiotemporal dynamics due to the collective behavior of dislocations [1−3]. At the same time, an unstable flow is a technologically important problem, since it unfavorably affects the formation of industrial metal alloys. In particular, strain localization in bands deteriorates the mechanical properties of structural materials and may cause their premature corrosion and sudden fracture. In addition, static or propagating deformation bands spoil the surface of industrial articles.

Most studies devoted to intermittent plastic flows were performed with a constant strain rate in a hard tensile testing machine, when it is manifested in stress drops (the Portevin−Le Chatelier (PLC) effect) [1−8]. The conditions of a constant increase in the stress rate in a soft tensile machine were used in a much smaller number of tests [4−6] despite that the first observations of stepwise plastic straining in these conditions were made in the second half of the 19th century. Intermittent creep was studied in a much smaller number of experiments than the PLC effect in metal alloys. Intermittent creep [7−10] manifests in the form of deformation steps with an amplitude of ~1−6% at the first and second creep stages; it was described in the literature as *sudden elongation, spontaneous straining,* or *strain burst.* In contrast to a constant strain rate and a constant (nonzero) stress growth rate, information on the step response on the creep curves (ladder creep) is extremely scarce.

At present, the problem of deformation macrosteps and the spatiotemporal patterns of deformation bands in the course of intermittent creep remain not quite clear in view of a comparatively small number of publications and the absence of these investigations over the last three decades. At the same time, an analysis of the mechanisms of intermittent creep and band formation is of great practical importance. In addition, considering the nonlinear dynamics, it is important to know the mechanism of spontaneous formation of spatiotemporal (dissipative) patterns of macroscopically localized plastic deformation under the conditions of a preset (controllable) external force, i.e., in a dynamically determined system.

This study is aimed at the in situ analysis of the critical conditions of formation of a macroscopic strain burst under the conditions of intermittent creep of the AlMg6 aluminum−magnesium alloy, the correlation between the force response to the evolution of a strain burst and the spatiotemporal structures of deformation bands, as well in investigation of transitions between different dynamic regimes of plastic instabilities and an analysis of the features of dynamic chaos and self-organized criticality.

1. EXPERIMENTAL TECHNIQUE

The material under investigation was the AlMg6 industrial aluminum−magnesium alloy (Al−6.15% Mg−0.65%Mn−0.25% Si−0.21%Fe−0.1% Cu−0.12% Zn wt %), which exhibits discontinuous flow in hard and soft testing machines [11, 12], including the creep conditions [13, 14]. Plane samples in the form of
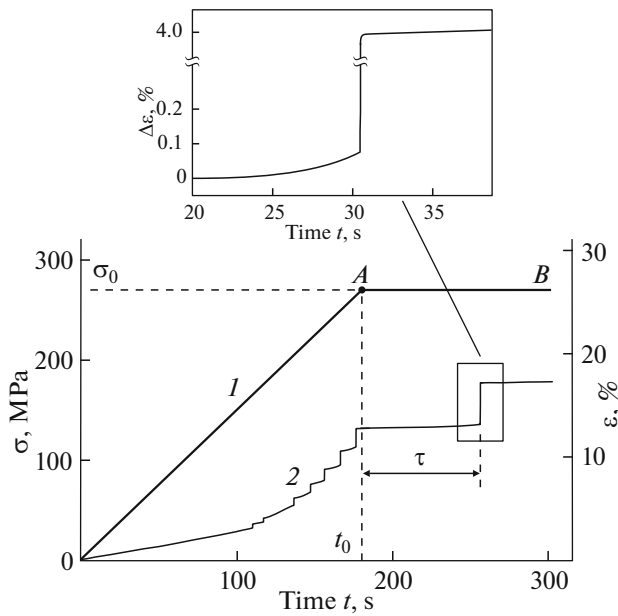
Fig. 1. Diagram of loading of a sample in a soft testing machine: (*1*) time dependence of applied stress $\sigma(t)$; *0A* is the active loading stage with a constant stress growth rate $\dot{\sigma}_0 = 1.5$ MPa/s TO fixed stress $\sigma_0 = 270$ MPa at $t_0 = 180$ s; *AB* is the creep stage, $\sigma_0 = $ const; (*2*) time dependence of strain $\varepsilon(t)$; τ is the incubation interval, i.e., the time of expectation of a strain burst in the creep regime. Inset shows the strain strain burst of amplitude $\Delta\varepsilon_m \approx 4\%$. Prior to the strain burst, the creep rate increases continuously analogously to the third creep stage.

double-sided blades with a working part size of 40 × 3 × 0.5 mm were machine-cut from a cold-rolled strip along the rolling direction. Prior to the test, the samples were annealed at 450°C for 1 h and quenched in air. After the thermal treatment, the average grain size was about 10 μm. The results of analyzing the microstructure were described in [15]. The complex of high-speed methods of detecting the strain, load, and analysis of the dynamics and morphology of deformation bands, as well as the scheme of tension in a soft testing machine were described in [13, 14].

2. RESULTS AND DISCUSSION

2.1. Critical Condition for the Formation of a Deformation Step during Creep

The samples were loaded in two consecutive stages, i.e., (i) loading stage at a constant rate $\dot{\sigma}_0 = 1.5$ MPa/s until the instant t_0 that corresponds to applied stress $\sigma_0 = (0.8–0.9)\sigma_u$ (Fig. 1, line *0A*), where $\sigma_u \approx 320$ MPa is the ultimate strength, and (ii) creep stage at engineering stress $\sigma_0 = $ const (Fig. 1, line *AB*). After time τ following the beginning of the creep stage, the sample loses stability, and the complex spatiotemporal deformation band structure spontaneously spreads over the sample surface along the direction of tension. It

should be emphasized that, immediately before the start of a strain burst, the continuous creep rate increases according to the power law $\dot{\varepsilon} = a\exp(bt)$ analogously to the behavior of the strain rate during the third creep stage (see inset to Fig. 1), where $a \approx 10^{-5}$ s^{-1} and $b \approx 0.3$ s^{-1} for applied stress $\sigma_0 = 270–280$ MPa, which considerably exceeds the conditional yield stress $\sigma_{0.2} \approx 155$ MPa and the critical stress corresponding to the first deformation step $\sigma_c \approx 165$ MPa at room temperature and stress rate $\dot{\sigma}_0 \sim 1–3$ MPa/s. In contrast to the conventional third state of continuous creep, the critical macroscopic event is not the fracture of the sample, but a strain burst, viz., a large step on the creep curve with an amplitude of several percent.

It was found that the strain burst begins at the instant when the continuous creep rate attains a certain critical value $\dot{\varepsilon}_{cr1} \sim 10^{-4}$ s^{-1}. Each next strain burst begins after additional sample loading with a stress of 5–10 MPa, when the rate of the preceding continuous creep attains critical value $\dot{\varepsilon}_{cr1}$ like the first strain burst. Therefore, the following empirical condition is determined for the beginning of the strain burst during continuous creep of AlMg6 alloy at room temperature: prior to the strain burst, the continuous creep rate varies over time from a constant dependence (like at the second creep stage) to a power dependence (like at the third stage) until the critical value $\dot{\varepsilon}_{cr1} \sim 10^{-4}$ s^{-1} is attained. It was found that the typical critical amplitude of strain burst in these testing conditions is ~1–6%, and the strain burst waiting time (incubation interval) is $\tau \sim 10–100$ s.

2.2. Correlation between the Deformation and Force Responses and the Deformation Band Dynamics

The data of video recording at a rate of 500 frames/s show that, as in the case of loading at a preset rate $\dot{\sigma}_0 = $ const [6], the strain burst under creep conditions for $\sigma_0 > \sigma_{0.2}$ begins simultaneously with the nucleation and subsequent expansion of the primary deformation band that has the form of an expanding neck inclined to the sample axis at an angle of about 60°. In the course of expansion, the band boundaries move antiparallel to that of the center of mass of the band remains unchanged. It was found that the broadening of the band consists of the following two sequential stages:

(i) The first (unloading) stage of very rapid broadening during 2–10 ms at a boundary velocity of ~10 cm/s, when the band width exceeds 90% of the final value (about 2 mm). This stage is accompanied by a deep stress drop with an amplitude of about 3–10 MPa.

(ii) The second (reloading) stage of slow broadening during a time interval of 10–100 ms with an average velocity of the boundary of about 3 mm/s. This

stage is accompanied by a partial or complete restoration of the stress.

Figure 2 shows a typical example of two-stage broadening of the deformation band. It can be seen that the durations of the first and second stages are 8 and 20 ms, respectively. In addition, the shape of the stress drop at the first stage correlates well with the time dependence of the band area $A(t) = [y_r(t) - y_l(t)]w(t)$, where $y_r(t)$ and $y_l(t)$ are the time dependences of the coordinates of the right and left boundaries of the band, respectively, and $w(t)$ is the sample width. At the reloading stage, the velocity of the band boundaries along the tension axis gradually decreases; when it attains the lower limit (~1 mm/s), the band boundaries generate bands at different instants with a time interval of 100−200 ms. The secondary bands are identical as a rule to the parent band and also have the form of expanding necks inclined at an angle of $55°−63°$ to the direction of tension. Then, the boundaries of the secondary bands generate the bands of the third generation, etc.

Figure 3 shows the results of synchronous recording of strain $\Delta\varepsilon$ and force response $\sigma(t)$ to the evolution of a deformation step with amplitude $\Delta\varepsilon_m$ of about 4% on the creep curve (Fig. 3, curves *1*, *2*). The video recording data obtained with a high speed of 2000 frames/s are processed in the form of the so-called correlation diagram, viz., time dependence $y(t)$ of the coordinates of the boundaries of deformation bands generated and broadened in the course of evolution of a strain burst. The main features of this correlation diagram were described in [14]. In particular, it was found that the correlation diagram consists of two branches separated by the point of inflection on the $\Delta\varepsilon(t)$ curve at which the strain rate is maximal ($\dot\varepsilon_m \approx 4 \times 10^{-2}\,s^{-1}$). The video recording data show that the macrolocalized strain appears near a sample blade and propagates first jumpwise like a type-*B* PLC band due to the token passing of the strain from one band (expanding neck) to another in accordance with the above-described mechanism, then (after the inflection point of the $\Delta\varepsilon(t)$ curve) quasi-continuously like a type-*A* PLC band that propagates to the opposite blade of the sample, reaching it at instant P (see curve *4* in Fig. 3). At the next instant F, a new band is generated near this blade, which moves in the opposite direction, demonstrating the opposite deformation behavior (first propagates continuously like a type-*A* band; then, after point D, it propagates discretely and jumpwise like a type-*B* band).

Let us consider the transitions between different dynamic regimes in greater detail in the evolution of an individual step on the creep curve. It should be noted that the instantaneous strain rate $\dot\varepsilon = \partial[\Delta\varepsilon(t)]/\partial t$ varies in a wide range from $\dot\varepsilon_{cr1} = 10^{-4}\,s^{-1}$ to $\dot\varepsilon_m \approx 10^{-2}\,s^{-1}$ during the evolution of a strain burst, and transitions occur between the behaviors of PCL bands of the B and A types; namely, plastic instability of type A is observed
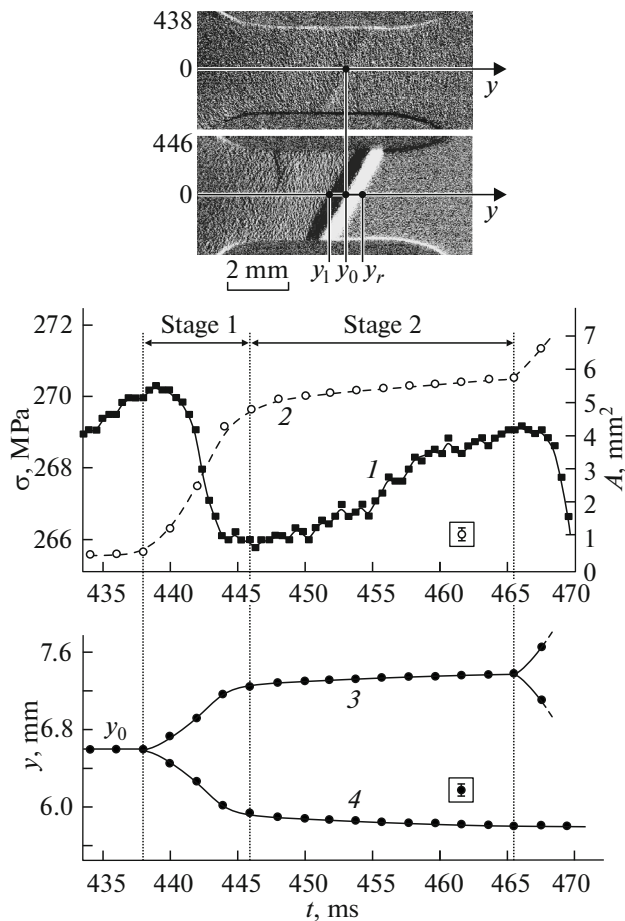

Fig. 2. Comparison of the time dependences of stress σ (*1*), area A (*2*) of the expanding deformation band, and coordinates y_r (*3*) and y_l (*4*) of the right and left boundaries of the deformation band. Horizontal arrows show the fast and slow stages (stages *1* and *2*, respectively) of expansion of the band. Inset shows the initial and final images of the expanding band at stage *1* from positions of generation (y_0) of the band and positions of the right (y_r) and left (y_l) boundaries of this band, respectively.

in the strain rate interval 2×10^{-2} to $4 \times 10^{-2}\,s^{-1}$. At the same time, if the strain rate of the sample decreases below $2 \times 10^{-2}\,s^{-1}$, the type-*A* instability is transformed into the *B*-type instability.

These results are in conformity with the conditions for the $B−A$ transitions in tests with a constant strain rate $\dot\varepsilon_0$ = const in hard tensile testing machines. It is known from the literature [16, 17] that a transition between different PLC regimes is controlled by a single scalar parameter, viz., strain rate $\dot\varepsilon_0$, which is kept constant during testing on a hard tensile testing machine. In particular, the $B−A$ transition in alloys of the Al−Mg system occurs in the interval ~10^{-3} to $10^{-2}\,s^{-1}$ (see [16−18]). In the case of intermittent creep of the AlMg6 alloy (see Fig. 3), the $B−A$ and then the $A−B$ transitions occur during the evolution of an individual strain burst, when the instantaneous strain rate
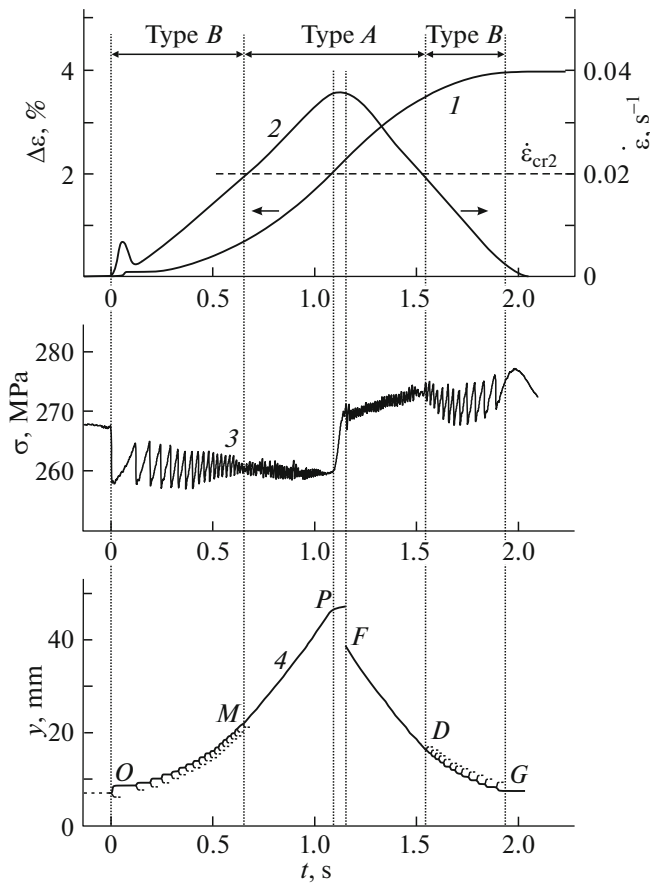
Fig. 3. Time dependences of strain increment $\Delta\varepsilon$ (*1*) and strain rate $\dot\varepsilon$ (*2*) developed during a strain burst, as well as force response σ (*3*) and coordinate y (*4*) of the boundaries of the bands (correlation diagram) in a sample of AlMg6 alloy for applied engineering stress $\sigma_0 = 268$ MPa. Vertical lines mark different types (*A* and *B*) of plastic instabilities. Horizontal dashed line indicates second critical strain rate $\dot\varepsilon_{cr2} \approx 2 \times 10^{-2}$ s^{-1} at which a transition between dynamic regimes *A* and *B* occurs.

of the sample passes through the second critical value $\dot\varepsilon_{cr2} \approx 2 \times 10^{-2}$ s^{-1}.

Let us now consider the dependence of true stress σ_{th} on true strain ε_{th} in the evolution of an individual strain burst under intermittent creep conditions. True stress σ_{th} and true strain ε_{th} are calculated using familiar expressions [19]

$$\sigma_{th} = \sigma(1 + \varepsilon), \qquad (1)$$

$$\varepsilon_{th} = \ln(1 + \varepsilon). \qquad (2)$$

The σ_{th} vs. ε_{th} curves are plotted to characterize the mechanical properties of materials under large strains in testing with a controllable constant strain rate ($\dot\varepsilon_0 =$ const) or with a constant stress growth rate ($\dot\sigma_0 =$ const). In the case of creep, the creep curve (time dependence of strain $\varepsilon(t)$) is usually constructed. However, in the conditions of intermittent creep, it is
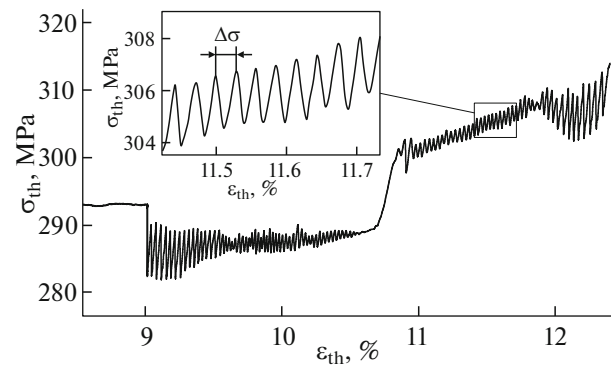
Fig. 4. Dependence of true stress σ_{th} on true strain ε_{th} obtained from the data of position and force sensor recording represented in Fig. 3 (curves *1* and *3*, respectively) in the course of evolution of the strain burst. Inset shows a fragment of this dependence and increment $\Delta\delta$ of the true strain between adjacent true stress drops.

expedient to plot the $\sigma_{th}(\varepsilon_{th})$ dependence to measure the true strain increment $\Delta\delta$ per deformation band. Figure 4 shows the σ_{th} vs. ε_{th} curve obtained by eliminating time from the temporal dependences of true stress $\sigma_{th}(t)$ and true strain $\varepsilon_{th}(t)$ calculated by formulas (1) and (2) from the results of measurements obtained using the force and strain sensors, i.e., from the $\sigma(t)$ and $\varepsilon(t)$ experimental curves (see Fig. 3, curves *3*, *1*) during the evolutions of a strain burst with an amplitude of 4%.

Figure 5 shows the histogram $n_i(\Delta\delta)$ of true strain increment $\Delta\delta$ between the nearest stress drops on the segment of the σ_{th} vs. ε_{th} curve corresponding to an individual strain burst. It can be seen from Figs. 4 and 5 that the strain increment almost remains unchanged during the evolution of a macroscopic strain burst and amounts to $\Delta\delta = (3.0 \pm 0.57) \times 10^{-2}\%$. Considering that each stress drop is found to be associated with the nucleation and broadening of a single deformation band, we can conclude that each such band carries nearly the same true strain; therefore, it can be treated as a quantum of the macrolocalized intermittent strain under the creep conditions.

2.3. Analysis of Nonlinear Oscillations in the Force Response during the Evolution of a Strain Burst

The above-described evolution of plastic instabilities in the course of macroscopic intermittent creep is an illustrative example of nonequilibrium morphogenesis, viz., spontaneous formation of complex spatiotemporal structures in an initially homogeneous and nonlinear media like effects of turbulence or dendrite solidification of a supercooled melt [20]. As noted above, time series $\sigma(t)$ consisting of numerous nonlinear oscillations (in the form of repetitive stress drops) is a complex force response of the sample–testing machine mechanical system to the spontaneous

evolution of a single macroscopic strain burst in creep conditions, when the external force acting on the system is maintained at a constant level. This intermittent time series, which maps the evolution of the spatio-temporal pattern of strain bursts onto one degree of freedom, makes it possible, first, to control the populations of deformation bands and the dynamic behavior of various types (*A* and *B*) directly in the course of straining and, second, to use the methods of statistical analysis of time series to analyze the effects of self-organization and dynamic chaos in the deformation behavior of a material.

2.3.1. Statistical analysis. It should be noted above all that, despite that an individual stress drop corresponds to approximately the same increment of the true strain, the amplitudes of true stress drops are distributed in a wide range of values of approximately 0.3—10 MPa, and the histogram of the stress drops has a nearly hyperbolic shape (Fig. 6a). In the log—log coordinates, the statistical distribution function $D(s) = N^{-1}dN/ds$ of the normalized stress drop amplitude $s = \Delta\sigma_{tr}/\sigma_{tr}$ is approximately linear with a slope of 1.87 to the s axis (see inset to Fig. 6a). (Here, σ_{tr} is the initial (prior to strain burst) level of the true stress, $\Delta\sigma_{tr}$ is the true stress drop, N is the total number of stress drops, and dN is the number of drops with amplitudes falling into the narrow interval $(s - \delta s/2, s + \delta s/2)$; see [21].) This means that the stress drop amplitude distribution function obeys the power law

$$D(s) \sim s^{-\alpha} \qquad (3)$$

with exponent $\alpha = 1.87$. It is known that the power distribution of the avalanche amplitudes with an exponent on the order of unity is typical of earthquakes (Guttenberg—Richter law [22]) and is a paradigm (to be more precise, a feature) of self-organized criticality (SOC).

It should be noted that the distribution of stress drop durations Δt_d also demonstrates a scaling form with exponent β as follows:

$$D(\Delta t_d) \sim \Delta t_d^{-\beta}. \qquad (4)$$

Normalized distribution $D(\Delta t_d)$ is shown in Fig. 6b in the log—log coordinates. The dashed line corresponds to exponent $\beta \approx 1.46$.

The normalized stress drop amplitude is connected with the stress drop duration by the power law

$$s \sim \Delta t_d^h. \qquad (5)$$

Figure 6c shows the dependence of log s on log Δt_d with exponent $h = 0.7$. According to [23], coefficients α, β and h obey the relation

$$\beta = h(\alpha - 1) + 1 \rightarrow 1.46 \approx 0.7(1.87 - 1) + 1 = 1.6. \qquad (6)$$

The scaling laws in Eqs. (3)—(5) and dimensionless relation (6) also indicate the self-organized criticality state [17, 23].
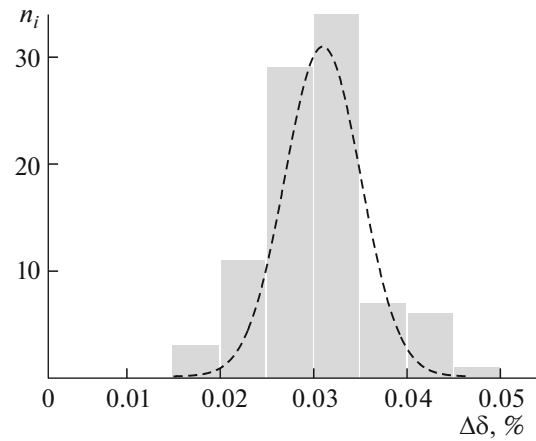
Fig. 5. Histogram $n_i(\Delta\delta)$ of the true strain increment between true stress drops.

In SOC notation, the term *criticality* indicates the existence of long-range correlations as in the case of the second-order phase transitions in the vicinity of the critical point [24]. Therefore, the results presented above clearly indicate the existence of strong spatial correlations of plastic instabilities in the course of intermittent creep.

According to [25, 26], the global dynamics for systems with SOC is assumed to be controlled by long-range correlations among a large number of local objects (nonequilibrium transfer carriers). According to the results of this study, these carriers are expanding deformation bands, i.e., quanta of macrolocalized strain, which form spatiotemporal structures whose dynamics corresponds to the behavior of PLC bands (of types *A* and *B*), and spatial correlation is governed by the token passing mechanism of propagation of the macrolocalized strain, in which each band (except the initial one) is formed at the boundary of the preceding band, where internal stresses exceed a certain threshold value.

2.3.2. Transitions between nonlinear dynamic regimes with self-organized criticality. The transitions between PLC dynamic regimes of the *A*, *B*, and *C* types were usually studied under the conditions of tension at a constant strain rate $\dot\varepsilon_0 = $ const in hard testing machines [16—18, 20, 21, 27, 28]. The traditional interpretation of transitions between these dynamic regimes upon a change in the strain rate is based on analyzing the competition between two characteristic times; time t_L of reloading between two successive stress drops and plastic relaxation time t_R for internal stresses. Since the rate sensitivity of the flow stress is negative in the region of the PLC effect, an increase in the strain rate leads to at least three consequences, i.e., (i) a decrease in the total stress level and, hence, an increase in the relaxation time associated with the thermoactivation motion of dislocations in the non-
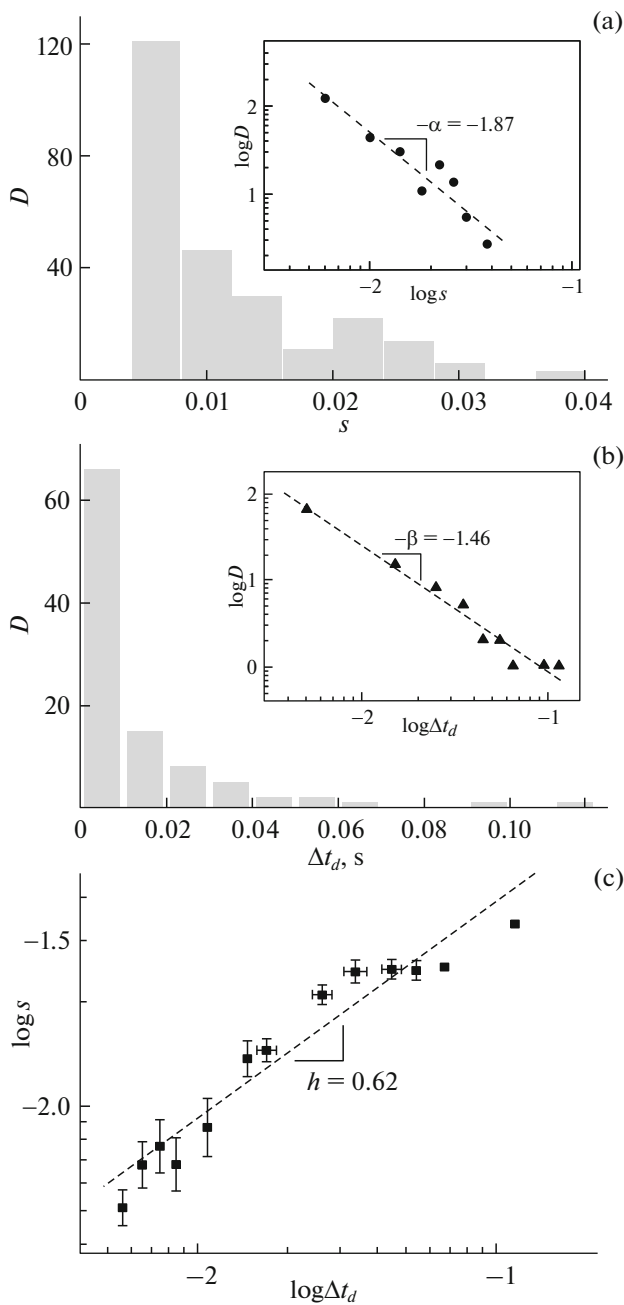
Fig. 6. Results of statistical analysis of the stress drops in the force response to the evolution of a strain burst in the creep conditions. (a, b) Densities of the distribution of normalized stress drop amplitude s and its duration Δt_d, respectively. Dashed lines show the negative slopes of these distributions in the log–log coordinates, which are equal to -1.87 and -1.46 for stress drop amplitudes and their durations, respectively; (c) dependence of s on Δt_d in the log–log coordinates. Dashed straight line indicates the power dependence of these quantities with exponent $h = 0.62$.

uniform field of internal stresses in the region of a deformation band; (ii) a decrease in the local strain rate drop in the band; and (iii) a decrease in the reloading time.

At a very low strain rate, the reloading time is very long, and $t_L \gg t_R$. Internal stresses are fully relaxed, and no spatial correlation between bands is observed. In the absence of spatial correlation, bands are formed in random positions in which the average stress attains the threshold value of instability nucleation, which leads to type-C behavior of the PLC effect. In early models of the PLC effect, spatial correlations were ignored, and the PCL dynamics was described exclusively in terms of relaxation oscillations [29] based on the concept of competition between dislocation pinning and depinning in the field of impurity atoms. In view of the random nature of the events associated with type-C sterss drops, the statistical distributions of stress drop amplitude and the intervals between them have the shape close to the Poisson distribution [16, 17]. With increasing strain rate, the time of reloading becomes shorter, while the plastic relaxation time increases. When these two quantities reach the same order of magnitude, internal stresses do not relax completely and facilitate the nucleation of new bands in the vicinity of pervious bands, which leads to jumpwise propagation of localized strain, associated with the B-type behavior of the PLC effect.

At high strain rates ($t_L \ll t_R$), only weak plastic relaxation can occur during stress restoration, which ensures a high degree of spatial correlation and quasicontinuous propagation of A-type bands. Internal stresses are always close to the critical value corresponding to the beginning of plastic instability so that many dislocation ensembles are close to the threshold of depinning from impurity ambience. As a result, the dislocation avalanches can be unpinned on any scale level and any time under the action of fluctuation of internal elastic stress fields. This leads to the power-law distributions of stress drops and intervals between them, which are free of the selected spatiotemporal scale. This situation is typical of systems that demonstrate the SOC state. The regime of crossover of type A and B dynamic regimes is expected for $t_L \sim t_R$ [17].

The pattern described above corresponds qualitatively to the structure of the force response during the evolution of a strain burst in the conditions of intermittent creep in the AlMg6 alloy. The main peculiarity is that the movable clamp in a soft tensile testing machine during the evolution of a strain burst in the intermittent creep conditions first develops a positive acceleration $\ddot{\varepsilon} > 0$ to the point of inflection, at which $\ddot{\varepsilon} = 0$ (point P in Fig. 3), then negative acceleration $\ddot{\varepsilon} < 0$ at the sharp deceleration stage. For this reason, instantaneous strain rate $\dot{\varepsilon}$ continuously increases in the time interval to point P, then decreases. When strain rate $\dot{\varepsilon}$ attains the critical value $\dot{\varepsilon}_{cr2} \approx 2 \times 10^{-2}$ s^{-1} (point M in Fig. 3), the reloading time t_L decreases to ~10 ms, while the unloading time equal to the duration of the stage of the very fast broadening of the deformation band (see Fig. 2) (i.e., plastic relaxation time t_R) increases from approximately 1.5 to 8 ms.

In the vicinity of the critical strain rate $\dot{\varepsilon}_{cr2}$, the reloading time is comparable with the characteristic plastic relaxation time ($t_L \approx t_R \approx 8-10$ ms), and the crossover of the B and A dynamic regimes is observed; namely, the jumpwise propagation of localized plastic deformation along the sample, which is accompanied by stress drops of type B with increasing frequency of drops is transformed into quasi-continuous spreading of a type A band with weak oscillations in force response $\sigma(t)$. Then, at the deceleration stage (when $\ddot{\varepsilon} < 0$), the strain rate $\dot{\varepsilon}$ continuously decreases, and the above pattern is scanned in the reverse sequence: a transition from dynamic regime A to regime B occurs near point D when the strain rate decreases to critical value $\dot{\varepsilon}_{cr2} \approx 2 \times 10^{-2}\,\text{s}^{-1}$ (Fig. 3) at which $t_L \approx t_R$.

As noted above, direct observations of the sample surface using a high-speed video camera have shown that in the type B dynamic regime, each band nucleates at the boundary of the preceding band. Consequently, the instability threshold is attained at the band boundary at which the strain gradient is maximal. This gradient induces elastic stresses that demonstrate incompatibility between the region plastically deformed by shear and the undeformed region of the material. When these stresses attain a critical value, e.g., the threshold stress of depinning of dislocations from the impurity ambient and/or the stresses of collective actuation of the Frank−Reed sources or their combination, the plastic relaxation of these elastic stresses due to the generation and broadening of the new deformation band takes place, which in turn leads to the evolution of the next stress drop in the force response in the inertial creep testing machine.

The strain rate of the entire sample varies over a relatively wide range (from $\dot{\varepsilon}_{cr} \sim 10^{-4}\,\text{s}^{-1}$ to about $4 \times 10^{-2}\,\text{s}^{-1}$) during the evolution of an individual strain burst. This leads to the rate scanning of different dynamic regimes (A and B). The resulting distribution of the stress drops is found to be of the power-law type, which indicates the tendency of the system to SOC. This conclusion is not surprising because the following basic conditions for the emergence of SOC are observed in the case of intermittent creep: (i) threshold dynamics (critical stress of depinning of dislocations from stoppers and/or collective actuation of the Frank−Reed sources, and so on); (ii) very slow external control relative to the rate of evolution of intrinsic events (in our case, local strain rates associated with a deformation band considerably exceed the overall strain rate of the sample, which precedes the evolution of a strain burst); (iii) the existence of two (fast and slow) time scales (t_L and t_R); and (iv) spatial coupling between defects, which probably appears in the form of internal stresses associated with the geometric incompatibility between adjacent regions of the material that strongly differ in the plastic strain level (gradient plasticity stresses).

Thus, the nonlinear dislocation dynamics in the course of macroscopic intermittent creep of the Al−Mg system is a new example of the self-organized criticality state. Note that the power-law statistics was observed for stress drops at low-temperature jumpwise deformation of niobium in a hard testing machine [30], for discrete events of acoustic emission of Al−Mg polycrystalline alloy deformed at a constant rate $\dot{\varepsilon}_0 = $ const under the conditions of the PLC effect [31, 32], as well as for amplitudes of the AE signals in the macroscopically continuous creep in ice single crystals [33] and electromagnetic emission signals in the case of uniaxial compression of ice, which is associated with the dynamics of dislocation avalanches and cracks during active loading in a soft machine [34].

In this work, in situ experiments were used to determine the mesoscopic mechanism of intermittent creep, which involves the spontaneous formation (during tenths of a second) of a complex spatiotemporal structure of deformation bands, which induces the evolution of a macroscopic step on the creep curve with an amplitude of up to 10%. The microscopic nature of intermittent creep remains not quite clear and requires further investigation.

CONCLUSIONS

The main results of this study can be formulated as follows.

1. Intermittent creep exhibits the threshold dynamics: a strain burst starts when the rate of the preceding continuous creep attains a certain critical value. The empirical conditions for the emergence of a strain burst in the AlMg6 alloy at room temperature have been determined. Prior to the strain burst, the creep rate changes from a constant value (as at the second creep stage) to the values increasing in accordance with a power law (as at the third creep stage) to critical value $\dot{\varepsilon}_{cr1} \sim 10^{-4}\,\text{s}^{-1}$.

2. Each stress drop in the structure of the force response correlates with a single mesoscopic deformation band in the form of an expanding neck inclined to the sample axis at an angle of about 60°. The evolution of the band is characterized by two consecutive (fast and slow) stages. At the slow stage, the velocity of the band boundaries gradually decreases, and when it drops to the lower limit (about 1 mm/s), the boundaries of secondary bands generate the third-generation bands, and so on. As a result of token passing of plastic deformation from one mesoband to another, when each band except the primary one is generated at the boundary of the preceding band, the macroscopically localized deformation propagates jumpwise along the direction of tension of the sample like a PLC macroscopic band of type B.

3. During the evolution of a strain burst, the strain rate varies in the interval from $\sim 10^{-4}$ to $4 \times 10^{-2}\,\text{s}^{-1}$, and a transition between the PLC regimes of types B

and A occurs when the strain rate passes through the second critical value $\dot{\varepsilon}_{cr2} \approx 2 \times 10^{-2}\ \mathrm{s}^{-1}$. These regimes are characterized by different levels of stress drop regularity in the force response.

4. It has been established that the temporal structure of the force response to the evolution of a macroscopic step on the creep curve demonstrates a tendency to the self-organized criticality state, which is a feature of a nonlinear behavior of the material in the intermittent creep conditions.

ACKNOWLEDGMENTS

REFERENCES

1. Y. Estrin and L. P. Kubin, *Continuum Models for Materials with Microstructures*, Ed. by H.-B. Mühlhaus (Wiley, New York, 1995), p. 395.
2. L. P. Kubin, C. Fressengeas, and G. Ananthakrishna, *Dislocations in Solids*, Ed. by F. R. N. Nabarro and M. S. Duesbery (Elsevier, Amsterdam, 2002), Vol. 11, p. 101.
3. E. Rizzi and P. Hahner, Int. J. Plast. **20**, 121 (2004).
4. J. F. Bell, *Experimental Foundations of Solid Mechanics; vol. 1: Mechanics of Solids*, Ed. by C. F. Truesdale (Springer, Berlin, 1973).
5. L. P. Kubin and Y. Estrin, Acta Metall. **33**, 397 (1985).
6. A. A. Shibkov and A. E. Zolotov, JETP Lett. **90**, 370 (2009).
7. E. N. da C. Andrade, Proc. R. Soc. A **84**, 1 (1910).
8. R. L. Klueh and J. F. King, Scr. Metall. **13**, 205 (1979).
9. R. L. Klueh and J. F. King, J. Nucl. Mater. **98**, 173 (1981).
10. G. Ananthakrishna and D. Sahoo, J. Phys. D: Appl. Phys. **14**, 2081 (1981).
11. A. A. Shibkov, A. A. Denisov, M. A. Zheltov, A. E. Zolotov, and M. F. Gasanov, Mater. Sci. Eng. A **610**, 338 (2014).
12. A. A. Shibkov, A. E. Zolotov, and M. A. Zheltov, Bull. Russ. Acad. Sci.: Phys. **76**, 85 (2012).
13. A. A. Shibkov, A. E. Zolotov, M. A. Zheltov, A. A. Denisov, and M. F. Gasanov, Tech. Phys. **59**, 508 (2014).
14. A. A. Shibkov, A. E. Zolotov, M. A. Zheltov, M. F. Gasanov, and A. A. Denisov, Phys. Solid State **56**, 889 (2014).
15. A. A. Shibkov, A. A. Mazilkin, S. G. Protasova, D. V. Mikhlik, A. E. Zolotov, M. A. Zheltov, and A. V. Shuklinov, Deform. Razrushenie Mater., No. 5, 24 (2008).
16. M. S. Bharathi, G. Ananthakrishna, C. Fressengeas, L. P. Kubin, and M. Lebyodkin, Phys. Rev. Lett. **87**, 165508 (2001).
17. M. S. Bharathi, M. Lebedkin, G. Ananthakrishna, C. Fressengeas, and L. P. Kubin, Acta Mater. **50**, 2813 (2002).
18. A. Chatterjee, A. Sarkar, P. Barat, P. Mukherjee, and N. Gayathri, Mater. Sci. Eng. A **508**, 156 (2009).
19. I. I. Novikov and V. K. Portnoi, *Superplasticity of Ultrafine-Grain Alloys* (Metallurgiya, Moscow, 1981).
20. D. A. Kessler, J. Koplik, and A. Levine, Adv. Phys. **37**, 255 (1988).
21. T. A. Lebedkina and M. A. Lebyodkin, Acta Mater. **56**, 5567 (2008).
22. B. Gutenberg and C. F. Richter, Ann. Geophis. **9**, 1 (1956).
23. J. Kertesz and B. L. Kiss, J. Phys. A: Math. Gen. **20**, L433 (1990).
24. E. M. Lifshitz and L. P. Pitaevskii, *Physical Kinetics* (Nauka, Moscow, 1979).
25. P. Bak, C. Tang, and K. Wiessenfeld, Phys. Rev. A: At., Mol., Opt. Phys. **38**, 364 (1988).
26. H. J. Jensen, *Self-Organized Criticality* (Cambridge Univ. Press, Cambridge, 1998).
27. I. V. Shashkov, M. A. Lebyodkin, and T. A. Lebedkina, Acta Mater. **60**, 6842 (2012).
28. M. Lebyodkin, Y. Brechet, Y. Estrin, and L. P. Kubin, Phys. Rev. Lett. **74**, 4758 (1995).
29. P. Penning, Acta Metall. **20**, 1169 (1972).
30. V. S. Bobrov, S. I. Zaitsev, and M. A. Lebedkin, Fiz. Tverd. Tela **32**, 3060 (1990).
31. M. Lebyodkin, Y. Brechet, Y. Estrin, and L. P. Kubin, Phys. Rev. Lett. **74**, 4758 (1995).
32. M. A. Lebyodkin and Y. Estrin, Acta Mater. **52**, 3403 (2005).
33. J. Weiss and J.-R. Grasso, J. Phys. Chem. B **101**, 6113 (1997).
34. A. A. Shibkov and A. A. Kazakov, Crystallogr. Rep. **54**, 299 (2009).

Translated by N. Wadhwa